



HAL
open science

Multifunctional Photovoltaic Window Layers for Solar-Driven Catalytic Conversion of CO₂: The Case of CIGS Solar Cells

Julian Guerrero, Elisabeth Bajard, Nathanaelle Schneider, Fabienne Dumoulin, Daniel Lincot, Umit Isci, Marc Robert, Negar Naghavi

► **To cite this version:**

Julian Guerrero, Elisabeth Bajard, Nathanaelle Schneider, Fabienne Dumoulin, Daniel Lincot, et al.. Multifunctional Photovoltaic Window Layers for Solar-Driven Catalytic Conversion of CO₂: The Case of CIGS Solar Cells. ACS Energy Letters, 2023, 8 (8), pp.3488-3493. 10.1021/acsenergylett.3c01205 . hal-04255937

HAL Id: hal-04255937

<https://cnrs.hal.science/hal-04255937v1>

Submitted on 24 Oct 2023

HAL is a multi-disciplinary open access archive for the deposit and dissemination of scientific research documents, whether they are published or not. The documents may come from teaching and research institutions in France or abroad, or from public or private research centers.

L'archive ouverte pluridisciplinaire **HAL**, est destinée au dépôt et à la diffusion de documents scientifiques de niveau recherche, publiés ou non, émanant des établissements d'enseignement et de recherche français ou étrangers, des laboratoires publics ou privés.

Multifunctional Photovoltaic Window Layers for Solar-driven Catalytic Conversion of CO₂: The Case of CIGS Solar Cells

Julian Guerrero,^{a,b} Elisabeth Bajard,^b Nathanaelle Schneider,^b Fabienne Dumoulin,^c Daniel Lincot,^b Umit Isci,^{d} Marc Robert,^{a,e*} Negar Naghavi^{b*}*

^a Laboratoire d'Electrochimie Moléculaire, Université Paris Cité, CNRS, F-75013 Paris, France

^b Institut Photovoltaïque d'Île-de-France (IPVF), CNRS, UMR 9006, 91120 Palaiseau, France

^c Acıbadem Mehmet Ali Aydınlar University, Faculty of Engineering and Natural Sciences, Biomedical Engineering Department, 34752 Ataşehir, Istanbul, Türkiye

^d Marmara University, Faculty of Technology, Department of Metallurgical & Materials Engineering, 34722 Istanbul, Türkiye

^e Institut Universitaire de France (IUF), F-75005, Paris, France

*Correspondence to umit.isci@marmara.edu.tr (U. Isci),

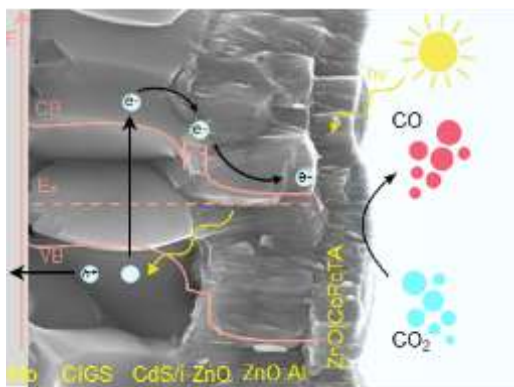
negar.naghavi@chimieparistech.psl.eu (N. Naghavi), robert@u-paris.fr (M. Robert)

ABSTRACT

Using a fast and simple one-step electrochemical method, we developed transparent and conductive ZnO nanoporous layers encapsulating molecular catalysts, showcasing dual functionality as a window layer for thin-film solar cells and a catalytic layer for solar-to-fuel conversion. As a proof of concept, tetra-ammonium substituted Co phthalocyanine (CoPcTA) was encapsulated into the window layer of high-efficiency Cu(In,Ga)Se₂ (CIGS) solar cells demonstrating photoelectrochemical (PEC) reduction of CO₂ into CO with a selectivity of 93% and current densities up to ca. 7 mA cm⁻² at -1.7 V vs SCE under 1 sun irradiation, which corresponds to a turnover number (TON) above 100,000 and a turnover frequency (TOF) of 10 s⁻¹ after 3h. The simplicity and versatility of this approach make the nanoporous catalytic ZnO layer not only easily adaptable to different high-efficiency solar cells but also pave the way for flexible testing of diverse molecular catalysts for CO₂ conversion into diverse, valuable fuels.

Keywords: Photoelectrochemical (PEC), carbon dioxide reduction, transparent conductive electrodes, molecular catalysts, solar cells, nanostructured materials

TOC GRAPHIC



Photovoltaics (PV) is currently one of the fastest-growing renewable industries. In this context, driving catalytic chemical reactions from PV using photoelectrochemical (PEC) approaches offers a sustainable mean of synthesizing chemicals and fuels while enabling the storage of intermittent solar energy. Efficient PV and solar-to-fuel technologies rely on semiconducting materials capable of converting sunlight into either direct current electricity or chemicals. In both cases, efficiency depends on the ability of the material to absorb light and generate charge carriers. The absorbers used for photovoltaic applications are excellent candidates as photoelectrodes, presenting high photocurrent due to their ability to absorb the major part of the visible light. However, these materials alone often lack sufficient energy to trigger the CO_2 reduction reaction (CO_2RR) and require high bias voltages or coupling with other materials.

In photovoltaics, the mechanism for charge carrier separation, based on *pn*-junction, generally outperforms the solid-liquid analog in terms of charge separation and electron transport.

In electrochemical CO_2RR , efficient catalysts are needed to facilitate multiple electron and proton transfers, achieving high current densities and selectivity. Molecular catalysis is very promising as atom-efficient catalysts with high intrinsic activities and tunable active sites are used.^{1,2} Such catalysts, with easily identifiable and tunable active sites, offer a variety of options for controlling the activity and product selectivity.¹

Encapsulating molecular catalysts directly within the window layers of PV solar cells, rather than grafting them onto additional layers like TiO_2 ,³⁻⁸ is an appealing approach. This eliminates the need for chemical modifications of catalysts and complex deposition processes, and simplifies manufacturing. The development of a transparent and conducting layer integrating efficient catalysts as a window layer on different PV solar cells holds numerous advantages, including enhanced performance, higher efficiency for charge transport to catalytic sites, as

well as better stability due to lower catalyst leaching, leading to the development of better-performing photocathode.

Most standard solar cells end-up at their front side by a transparent and conducting layer, such as ZnO:Al, In₂O₃:Sn (ITO) or SnO₂:F (FTO), called window layer.⁹⁻¹² This paper discusses the development of a transparent and conductive nanoporous ZnO layer encapsulating a molecular catalyst for use as a front contact layer in Cu(In,Ga)Se₂ (CIGS) solar cells. CIGS is a promising PV thin film technology known for its high efficiency, stability, and low manufacturing cost. CIGS-based solar cells have achieved a record efficiency of 23.6%.¹³ Because of its direct bandgap and high absorption coefficient ($\alpha = 10^7 - 10^8 \text{ m}^{-1}$ in the visible region, Figure S1), the CIGS alloy is a high-performance absorber material where only 1 to 2 μm are required to absorb the maximum number of photons. In these solar cells, *p*-type polycrystalline CIGS is deposited on a soda lime glass covered with molybdenum (Mo), forming a heterojunction with a CdS layer and an *i/n*-ZnO:Al front contact (Figure S2).

The nanoporous ZnO layer serves multiple functions, acting as a front contact and protective layer for the solar cell and adding catalytic activity to the CIGS photoelectrode for solar-to-fuel conversion. ZnO is chosen for its unique advantages, such as being easily prepared in high quality and in various structures and shapes¹⁴⁻¹⁷ using solution routes like electrodeposition.^{18,19} The solution environment promotes self-assembly structures, and the nanostructured architecture of ZnO facilitates the movement of electrons and holes due to quantum confinement.

In the optimization process, a standard CIGS cell absorber with a bandgap of 1.2 eV was used in a standard configuration of glass/Mo/CIGS/CdS/*i*-ZnO/ZnO:Al. A water-soluble tetracationic Co phthalocyanine complex, (Figure S3) was encapsulated into the nanoporous ZnO layer during its photo-electrodeposition on the ZnO:Al window layer of the CIGS solar cells. The thickness of the ZnO|CoPcTA nanoporous (ZnO|CoPcTA NP) layer and the concentration of the catalyst could be controlled by adjusting the transferred charge during the ZnO growth process as observed on Figure 1a.²⁰ Increasing the charge from 0 to 4 C cm⁻² results in a relatively linear increase in ZnO|CoPcTA NP thickness up to 1200 nm. SEM cross-section images of Mo/CIGS/CdS/*i*-ZnO/ZnO:Al/ZnO|CoPcTA NP cells (Figures 1b-c) reveal that the top nanoporous layer presents a fibrous internal nanostructure aligned in the direction of film growth, which is consistent with similar ZnO/organic layers developed in the literature.^{18,21} The top view SEM images confirm the change in morphology, with the ZnO|CoPcTA NP window

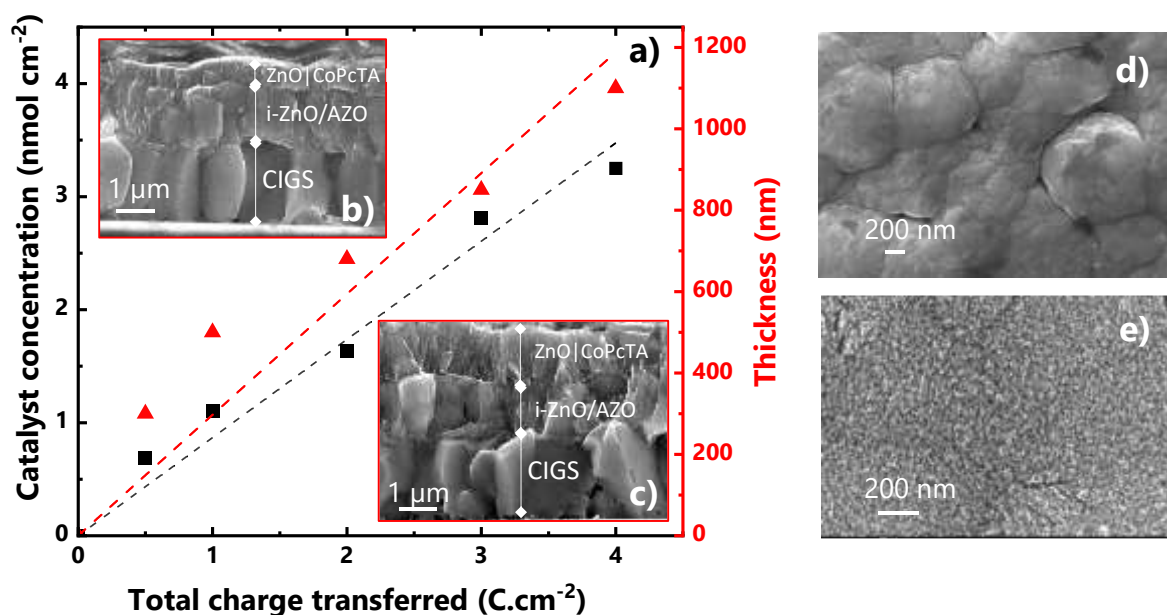


Figure 1 (a) ZnO|CoPcTA NP layer thickness (as determined from SEM images, red triangles) and CoPcTA concentration (in nmol cm⁻², quantified by ICP analysis, black squares) as a function of the total charge transferred during the electrodeposition (in C.cm⁻²). (b, c) Cross section SEM images of the modified Mo/CIGS/CdS/i-ZnO/ZnO:Al electrodes upon adding ZnO|CoPcTA NP layers of 500 and 1100 nm respectively. (d, e) Top view SEM images of the Mo/CIGS/CdS/i-ZnO/ZnO:Al electrodes before and after addition of the ZnO|CoPcTA NP layer respectively.

layer exhibiting a sponge-like porous surface compared to the dense sputtered ZnO thin film (Figure 1d-e). Inductively coupled plasma optical emission spectrometry (ICP-OES) on ZnO|CoPcTA NP samples confirmed the incorporation of the molecular catalyst into the electrodeposited layers. Measurements show that the concentration of the CoPcTA molecule in the layers is linearly correlated to the film thickness and the catalyst concentration remains in the order of a nanomol per square centimeter (from 0.5 to 3.6 nmol cm⁻², Figure 1a).

The ZnO|CoPcTA NP layers were subjected to detailed analysis using X-ray Photoelectron Spectroscopy (XPS, Figure S4), Energy Dispersive X-ray Spectroscopy (EDX, Figure S5), Fourier Transform Infrared Spectroscopy (FTIR, Figure S6) and Atomic Force Microscopy (AFM, Figure S9). They confirmed that the CoPcTA catalyst is effectively incorporated and uniformly dispersed within the ZnO layer, without any observed aggregation of cobalt. Comparisons between the X-ray diffraction patterns of the sputtered-ZnO:Al substrate and the ZnO|CoPcTA NP layer (Figure S7) revealed that both layers exhibit a well-crystallized ZnO

wurtzite type structure. The highly preferred orientation along the (002) direction confirms the internal crystalline quality of the layer which can favor electron transport properties.

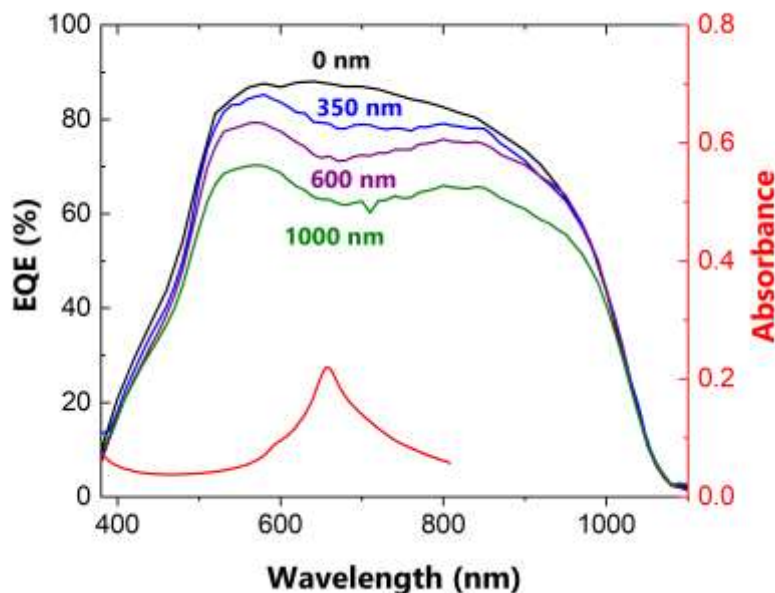


Figure 2 External Quantum efficiency (EQE) of CIGS solar cells covered with ZnO|CoPcTA NP layers with thicknesses from 0 to 1000 nm compared with the absorbance spectra of 50 μM of CoPcTA molecule in aqueous solution.

The impact of hybrid nanoporous layers on the performance of CIGS solar cells was evaluated through J-V measurements under 1 sun illumination (100 mW cm^{-2} AM 1.5G). The thickness of the ZnO|CoPcTA NP layer ranges from 0 to 1000 nm. The efficiency, fill factor (FF), open circuit voltage (V_{OC}), and short circuit current density (J_{SC}) of the solar cells were compared to a non-modified CIGS solar cell (Table 1). Increasing the thickness of the ZnO|CoPcTA NP layers up to 1000 nm primarily affects the J_{SC} and FF of the cells. J_{SC} decreases from 33.9 mA cm^{-2} to 27.2 mA cm^{-2} , and FF from 75% to 67%, resulting in a slight decrease in V_{OC} from 698 mV to 633 mV. Consequently, the efficiency of the modified CIGS cells diminishes from 17.8% to 9.0% for ZnO|CoPcTA NP layer thicknesses up to 1000 nm. The diminution in FF can be attributed to the introduction of a new layer, which creates additional interfaces, leading to losses in electron transport and recombination facilitation. The lower J_{SC} may be due to lower transmission of the ZnO|CoPcTA NP layers compared to standard ZnO:Al layers in the visible wavelength range. However, even with a 1000 nm thick nanoporous layer, current densities of up to 27 mA cm^{-2} can still be achieved. The external quantum efficiency (EQE) measurements

(Figure 2) showed a decrease in the EQE curves, particularly in the wavelength region between 550 nm and 850 nm, as the thickness of the ZnO|CoPcTA NP layers increased. This corresponds to the absorbance region of the CoPcTA molecule, explaining the reduction in the number of electrons produced in that wavelength region.

Table 1 J-V parameters of the modified CIGS cells.

Sample	J_{sc} (mA cm^{-2})	V_{oc} (mV)	FF (%)	η (%)
CIGS cell	33.9	698	75	17.8
CIGS cell+ ZnO CoPcTA NP 350 nm	31.4	685	71	15.8
CIGS cell+ ZnO CoPcTA NP 600 nm	29.3	663	67	12.1
CIGS cell+ ZnO CoPcTA NP 1000 nm	27.2	633	67	9.0

To enable solar-to-fuel applications, the hybrid layer added to the CIGS device needs to be thin enough to allow light transmission while containing an adequate catalyst amount for catalytic activity. After conducting several tests, a ZnO|CoPcTA NP layer with a thickness of 350 nm was selected for subsequent experiments, so as to favor high photovoltaic efficiency for PEC- CO_2 reduction while minimizing current losses.

To investigate the CO_2 reduction activity of the modified CIGS device under PEC conditions, linear sweep voltammetry (LSV) experiments were performed under chopped AM 1.5G illumination in a 0.1 M TBAPF₆ acetonitrile solution with 1% and 2% water as a proton source, saturated with either Ar or CO_2 (Figure 3a). The addition of a proton source was found to enhance the catalytic performance of the ZnO|CoPcTA NP layers,²⁰ most likely by accelerating CO_2 protonation and C-O bond cleavage^{23,24,25} along with the overall reaction:



On Figure 3a, upon saturating the solution with Argon, a small cathodic current is observed, attributed to the hydrogen evolution reaction, reaching around -2.4 mA cm^{-2} at -2.1 V vs. SCE . Upon CO_2 saturation, a current density of ca. -12.5 mA cm^{-2} was measured at -2.1 V vs. SCE , with a photogenerated current difference (j_{ph}) of up to 7 mA cm^{-2} between dark and illuminated

current. Increasing the water concentration to 2% significantly enhanced the current density, reaching a maximum value of approximately -16.2 mA cm^{-2} at -2.1 V vs. SCE , with a photogenerated current of around -9.3 mA cm^{-2} . Further increasing the water concentration did not have a significant effect on the current density but promoted a higher production of hydrogen and faster degradation of the photoelectrode. The maximum current density achieved (-16.2 mA cm^{-2} at -2.1 V vs. SCE) is higher than previously reported results in organic solvents²² but lower than the expected performance based on the CIGS solar cell characteristics ($J_{\text{SC}} \sim 31 \text{ mA cm}^{-2}$) reported in Table 1. This lower photocurrent may be attributed to carrier recombination at different stages of the process.

In Figure 3b, the LSV of a CIGS solar cell (Mo/CIGS/CdS/i-ZnO/ZnO:Al) and a modified CIGS electrode with an additional ZnO|CoPcTA NP layer are compared in the dark and under illumination (100 mW cm^{-2}). The modified CIGS electrode reached a current density of -8.3 mA cm^{-2} at -1.8 V , compared to the non-modified CIGS cell reaching -1.0 mA cm^{-2} at the same potential. This demonstrates the improved catalytic performance upon ZnO|CoPcTA NP layer incorporation. On the same curve, the illuminated Mo/CIGS/CdS/i-ZnO/ZnO:Al/ZnO|CoPcTA electrode achieved a current density of -0.5 mA.cm^{-2} at a slightly negative potential of -0.95 V vs. SCE . However, in the dark, the same current density required a high overpotential of -1.47 V vs. SCE . Upon illumination, the Mo/CIGS/CdS/i-ZnO/ZnO:Al/ZnO|CoPcTA NP cathode presents a photovoltage of ca. 0.5 V , this value being slightly lower to the V_{OC} delivered by the CIGS solar cell (Table 1). Although a fraction of the incident light is absorbed by the ZnO|CoPcTA NP top layer of the solar cell, the majority of photons penetrate through and successfully reach the CIGS/CdS *pn*-junction. These photons generate electrons that are then transported to the catalytic centers of the hybrid layer. The higher photocurrents observed in Mo/CIGS/CdS/i-ZnO/ZnO:Al/ZnO|CoPcTA NP electrodes compared with standard CIGS solar cells demonstrate the improved catalytic performance of the system thanks to the incorporation of a layer of ZnO hybrid molecular catalyst on top of the CIGS solar cells.

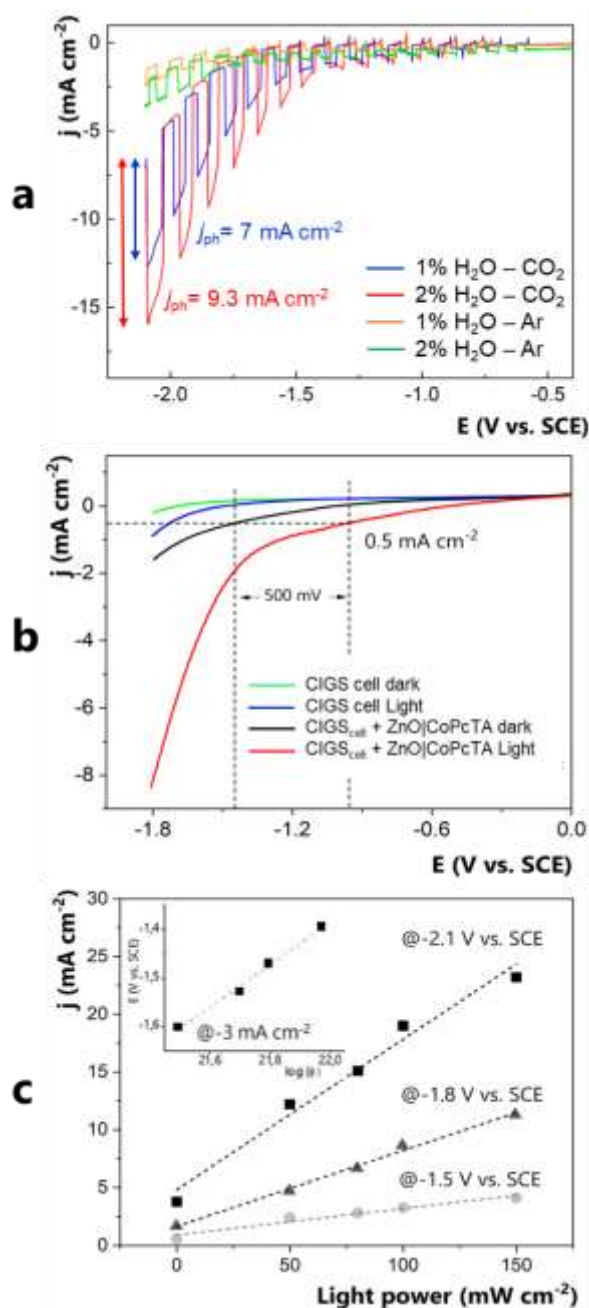


Figure 3 (a) Linear sweep voltammograms under chopped illumination (100 mW cm^{-2}) of a Mo/CIGS/CdS/i-ZnO/ZnO:Al + ZnO|CoPcTA NP (350 nm) photoelectrode under Ar or CO_2 saturated 0.1 M TBAPF_6 acetonitrile solution, with water concentration ranging from 1 to 2%. The scan rate was 100 mV s^{-1} . (b) Linear sweep voltammograms of a Mo/CIGS/CdS/i-ZnO/ZnO:Al photoelectrode compared to a Mo/CIGS/CdS/i-ZnO/ZnO:Al + ZnO|CoPcTA NP (350 nm) photoelectrode in the dark and upon illumination (100 mW cm^{-2}) in CO_2 saturated 0.1 M TBAPF_6 and $2\% \text{ H}_2\text{O}$ acetonitrile solution. Scan rate 100 mV s^{-1} . (c) Current density as a function of the light power, measured at -2.1 , -1.8 and -1.5 V vs. SCE respectively. Inset: Potential applied to reach a current density of 3.0 mA cm^{-2} as a function of the incident flux ($\log \Phi_0$).

To understand the relationship between photon flux, photocurrent, and photovoltage, we studied the impact of light power on photocurrent in the modified CIGS electrodes of the PEC CO₂ reduction system. Figure 3c displays the current density variation as light power ranges from 0 to 150 mW cm⁻². In solar cells, photocurrent (J_{tot}) is directly proportional to the absorbed photon flow (Φ_0): $J_{\text{tot}} \approx q\Phi_0$. Thus, the current density increases linearly with higher light power intensity. Additionally, Figure 3c inset demonstrates that for a current density of -3 mA cm⁻², the potential is logarithmically proportional to the incident flux (Φ_0). This is the expected behavior of a solar cell under normal conditions, indicating that the modified device with the ZnO|CoPcTA NP layer maintains a strong photovoltaic response even after the light-assisted electrodeposition process. The linearity suggests that the electro-catalysis process is not limited by CO₂ or proton diffusion but rather by the absorbed photons converted into electron-hole pairs. Upon increasing the light power up to 150 mW cm⁻², current densities up to 22.7 mA cm⁻², -11.2 mA cm⁻² and -4.5 mA cm⁻² at -2.1, -1.8 and -1.5 V vs SCE were respectively obtained.

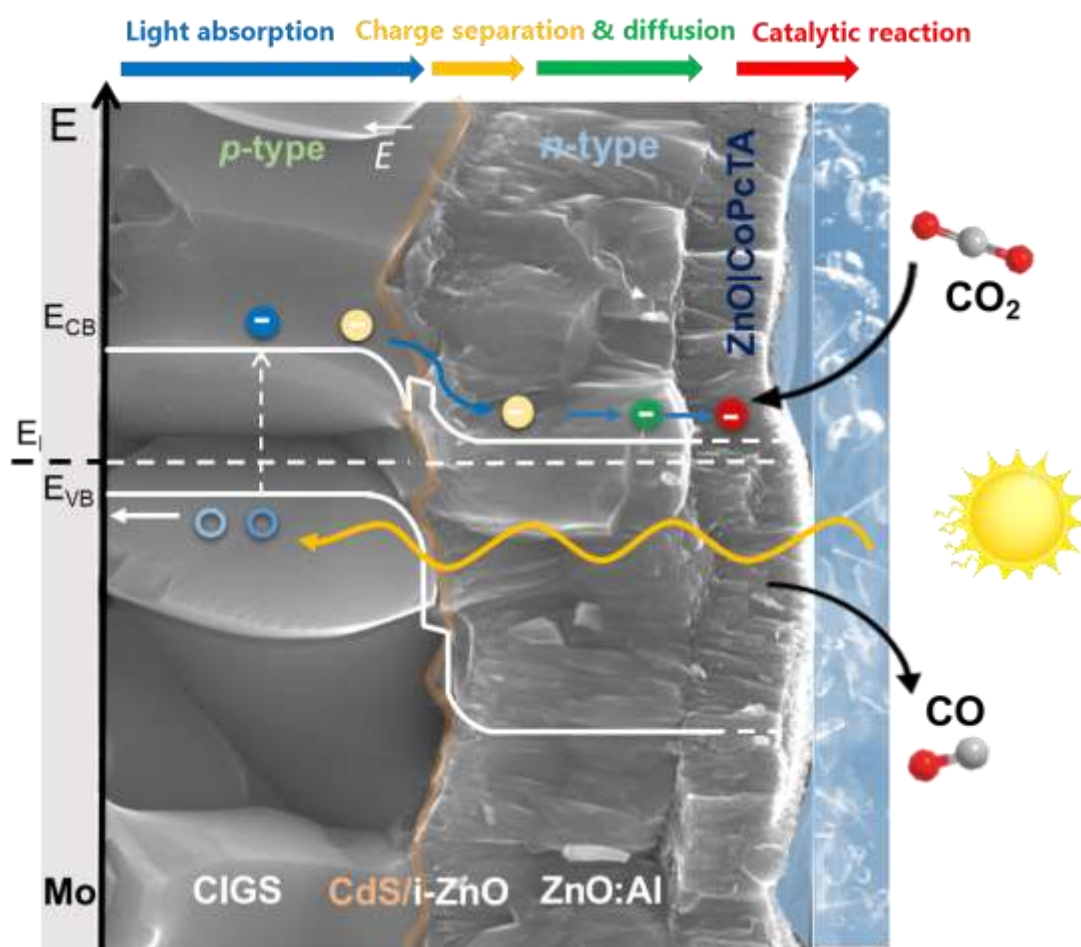


Figure 4 Schematic representation of a Mo/CIGS/CdS/i-ZnO/ZnO:Al photoelectrode covered with a ZnO|CoPcTA NP layer.

The mechanism for CO₂ reduction over CIGS solar cells can be summarized as follows (Figure 4). When illuminated, incoming photons generate electron-hole pairs within the CIGS absorbers. The *pn*-junction between CIGS and CdS facilitates the separation and collection of these charges. The electric field across the *pn*-junction directs electrons from the p-type absorber to the n-type buffer layer and further transports them through the highly conducting ZnO:Al window layer. These electrons eventually reach the ZnO|CoPcTA NP layer, where they are directed to the incorporated molecular catalyst to facilitate the electrochemical CO₂ reduction reaction. However, increasing the thickness of the nanoporous layer, while increasing the quantity of catalysts, negatively impacts the J_{SC} and FF of the solar cells. Since a part of the electronic transport occurs between the ZnO nanoporous, the catalysts and the electrolyte, part of the photogenerated electrons may accumulate in the ZnO layer or be recombined at the ZnO/molecular catalysis interface.²⁶

Figure 5a demonstrates the PEC CO₂ reduction under 100 mW cm⁻² illumination using different electrode stacks: a standard CIGS solar cell, a CIGS solar cell with a hybrid ZnO|CoPcTA NP, and a pure CoPcTA molecule loaded on a carbon electrode. All chronoamperometry experiments were conducted at a constant potential of -1.5 V vs SCE for a minimum of 3 hours. By adding a 350 nm thick nanoporous ZnO layer encapsulating only 0.75 nmol cm⁻² of CoPcTA,

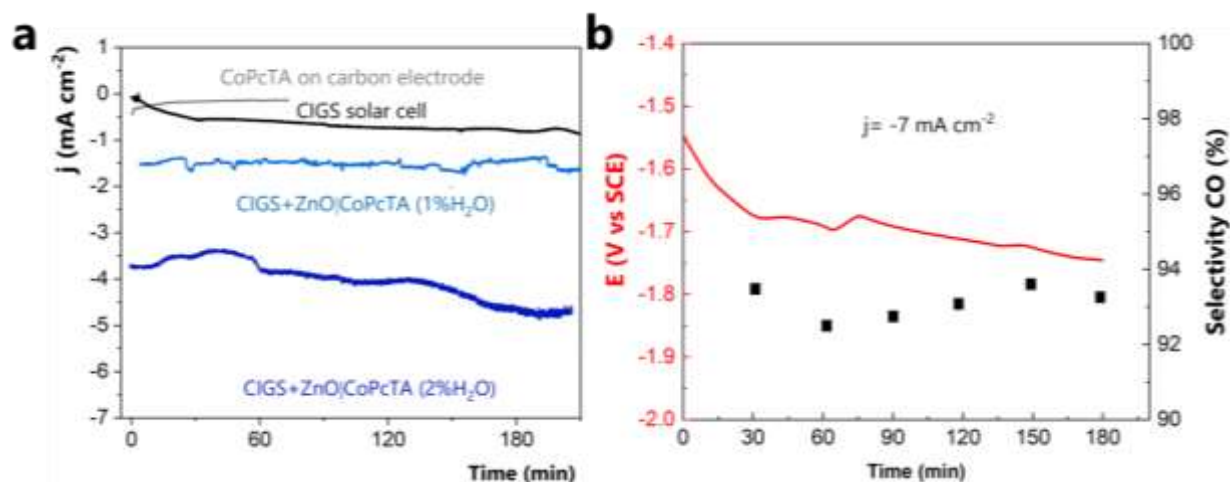


Figure 5 Chronoamperometry of CIGS photocathodes for PEC CO₂ reduction in CO₂ saturated 0.1 M TBAPF₆ acetonitrile solution. (a) Comparison of CO₂ electrolysis using CoPcTA loaded on carbon electrode with PEC CO₂ reduction using a standard CIGS cell and a modified CIGS cell with a ZnO|CoPcTA NP (350 nm) window layer at -1.5 V vs. SCE. (b) Potential of the electrode and selectivity for a constant current density held at -7 mA cm⁻², using a Mo/CIGS/CdS/i-ZnO/ZnO:Al + ZnO|CoPcTA NP (350 nm) photoelectrode adding 2 % H₂O. Electrodes surface: 0.5 cm². Light power: 100 mW cm⁻².

the CIGS system achieves significant catalytic CO₂ reduction with 94% selectivity, sustaining high current densities of around 4 mA cm⁻² for at least 3 hours, H₂ was the only by-product detected. The incorporation of molecular catalysts enhances the photoelectrode's current densities, achieving four times higher values compared to a standard CIGS solar cell.

To evaluate the performance and stability of a photoelectrode under higher current densities than -4 mA cm⁻², a PEC CO₂ reduction experiment was conducted at current density of -7 mA cm⁻² (Figure 5b) using the best electrolyte conditions: a CO₂-saturated 0.1 M TBAPF₆ and 2% H₂O acetonitrile solution. The high current density was sustained for 3 hours. The initial potential value was approximately -1.55 V vs. SCE, gradually shifting to around -1.70 V vs. SCE. Under these conditions, the system consistently produced -7 mA cm⁻² with an average CO selectivity of approximately 93%, corresponding to a partial current density for CO production (j_{CO}) of ca. -6.5 mA cm⁻², only obtaining 8% of H₂ as the by-product, a turnover number (TON) above 100,000 and a turnover frequency (TOF) of 10 s⁻¹ (see Supporting Information). Figure S9 demonstrates the long-term stability of a Mo/CIGS/CdS/i-ZnO/ZnO:Al + ZnO|CoPcTA photoelectrode (350 nm) during PEC CO₂ reduction at an applied potential of -1.45 V vs. SCE over 10h. The current density of the photoelectrode remains relatively stable throughout the experiment, with a slight decrease from -1.6 to -1.27 mA cm⁻², and CO selectivity close to 92% throughout the entire experiment.

In summary, our study introduces a versatile functional window layer that encapsulates molecular catalysts, achieving high catalytic activity with minimal use of molecular materials and a straightforward preparation method. These functional window layers were easily integrated onto high-efficiency CIGS-based solar cells within only a few minutes, using a light-assisted electrodeposition process. The resulting Mo/CIGS/CdS/i-ZnO/ZnO:Al/ZnO|CoPcTA NP stack presents a current density of up to -7 mA cm⁻² at -1.7 V vs SCE for 3 hours under visible light irradiation in an acetonitrile solution, with a CO selectivity >92%. This remarkable performance can be attributed to the combined effects of the catalytic properties of the hybrid layer comprising ZnO and CoPcTA molecular catalyst, efficient light harvesting of the CIGS material, rapid charge transport within the CIGS cell layers, enabling electron transfer to the catalytic centers in the outermost layer, and swift CO₂ reduction at the catalytic sites. Furthermore, by slightly increasing the light intensity to 150 mW cm⁻², we achieved current densities of up to 22 mA cm⁻² at -2.1 V vs SCE in an organic solvent, surpassing state-of-the-art PEC CO₂RR systems employing co-catalysts' (Table T-S1). This approach offers versatility, as it can be applied to various high-efficiency solar cells, providing flexibility to test a large set

of molecular catalysts without performing chemical modification. Additionally, it offers the potential for enhanced visible light absorption and improved catalytic efficiency of PEC systems.

ASSOCIATED CONTENT

Supporting Information Available.

Experimental data to support the results of the main text (experimental details, XPS, EDX, ATR-IR, AFM, XRD, long-term PEC experiment, product quantification, and comparison among state-of-the-art photocathodes for PEC CO₂ reduction in various solvents).

AUTHOR INFORMATION

Corresponding Authors

Umit Isci – Marmara University, Faculty of Technology, Department of Metallurgical & Materials Engineering, 34722 Istanbul, Türkiye; <https://orcid.org/0000-0002-6285-0524>;

Email: umit.isci@marmara.edu.tr

Negar Naghavi – Institut Photovoltaïque d'Île-de-France (IPVF), CNRS, UMR 9006, 91120 Palaiseau, France; <https://orcid.org/0000-0002-6045-5096>;

Email: negar.naghavi@chimieparistech.psl.eu

Marc Robert – Université Paris Cité, Laboratoire d' Electrochimie Moléculaire, CNRS, F-75013 Paris, France; Institut Universitaire de France (IUF), F-75005 Paris, France; <https://orcid.org/0000-0001-7042-4106>;

Email: robert@u-paris.fr

Authors

Julian Guerrero – Université Paris Cité, Laboratoire d' Electrochimie Moléculaire, CNRS, F-75013 Paris, France; Institut Photovoltaïque d'Île-de-France (IPVF), CNRS, UMR 9006, 91120 Palaiseau, France.

Elisabeth Bajard – Institut Photovoltaïque d'Île-de-France (IPVF), CNRS, UMR 9006, 91120 Palaiseau, France.

Nathanaelle Schneider – Institut Photovoltaïque d'Île-de-France (IPVF), CNRS, UMR 9006, 91120 Palaiseau, France; <https://orcid.org/0000-0001-7749-2400>.

Fabienne Dumoulin – Acıbadem Mehmet Ali Aydınlar University, Faculty of Engineering and Natural Sciences, Biomedical Engineering Department, 34752 Ataşehir, Istanbul, Türkiye; <https://orcid.org/0000-0002-0388-8338>.

Daniel Lincot– Institut Photovoltaïque d’Île-de-France (IPVF), CNRS, UMR 9006, 91120 Palaiseau, France.

Author Contributions

The manuscript was written through contributions of all authors. All authors have given approval to the final version of the manuscript.

Notes

The authors declare no competing financial interest.

ACKNOWLEDGEMENTS

The authors are very grateful for the financial support from the CNRS through the 80|Prime program. M.R. acknowledges the Institut Universitaire de France (IUF) for partial financial support. The authors thank NICE Solar Energy GmbH for supplying the solar cells used in this work.

REFERENCES

- (1) Dalle, K. E.; Warnan, J.; Leung, J. J.; Reuillard, B.; Karmel, I. S.; Reisner, E. Electro- and Solar-Driven Fuel Synthesis with First Row Transition Metal Complexes. *Chem. Rev.* **2019**, *119* (4), 2752–2875. <https://doi.org/10.1021/acs.chemrev.8b00392>.
- (2) Zhang, B.; Sun, L. Artificial Photosynthesis: Opportunities and Challenges of Molecular Catalysts. *Chem. Soc. Rev.* **2019**, *48* (7), 2216–2264. <https://doi.org/10.1039/C8CS00897C>.
- (3) Leung, J. J.; Warnan, J.; Ly, K. H.; Heidary, N.; Nam, D. H.; Kuehnel, M. F.; Reisner, E. Solar-Driven Reduction of Aqueous CO₂ with a Cobalt Bis(Terpyridine)-Based Photocathode. *Nat. Catal.* **2019**, *2* (4), 354–365. <https://doi.org/10.1038/s41929-019-0254-2>.
- (4) Roy, S.; Miller, M.; Warnan, J.; Leung, J. J.; Sahn, C. D.; Reisner, E. Electrocatalytic and Solar-Driven Reduction of Aqueous CO₂ with Molecular Cobalt Phthalocyanine–Metal Oxide Hybrid Materials. *ACS Catal.* **2021**, *11* (3), 1868–1876. <https://doi.org/10.1021/acscatal.0c04744>.
- (5) Schreier, M.; Gao, P.; Mayer, M. T.; Luo, J.; Moehl, T.; Nazeeruddin, M. K.; Tilley, S. D.; Grätzel, M. Efficient and Selective Carbon Dioxide Reduction on Low Cost Protected Cu₂O Photocathodes Using a Molecular Catalyst. *Energy Environ. Sci.* **2015**, *8* (3), 855–861. <https://doi.org/10.1039/C4EE03454F>.
- (6) Schreier, M.; Luo, J.; Gao, P.; Moehl, T.; Mayer, M. T.; Grätzel, M. Covalent Immobilization of a Molecular Catalyst on Cu₂O Photocathodes for CO₂ Reduction. *J. Am. Chem. Soc.* **2016**, *138* (6), 1938–1946. <https://doi.org/10.1021/jacs.5b12157>.
- (7) Pati, P. B.; Wang, R.; Boutin, E.; Diring, S.; Jobic, S.; Barreau, N.; Odobel, F.; Robert, M. Photocathode Functionalized with a Molecular Cobalt Catalyst for Selective Carbon Dioxide Reduction in Water. *Nat. Commun.* **2020**, *11* (1), 3499. <https://doi.org/10.1038/s41467-020-17125-4>.

- (8) Liu, J.; Shi, H.; Shen, Q.; Guo, C.; Zhao, G. Efficiently Photoelectrocatalyze CO₂ to Methanol Using Ru(II)-Pyridyl Complex Covalently Bonded on TiO₂ Nanotube Arrays. *Applied Catalysis B: Environmental* **2017**, *210*, 368–378. <https://doi.org/10.1016/j.apcatb.2017.03.060>.
- (9) Koida, T.; Fujiwara, H.; Kondo, M. Hydrogen-Doped In₂O₃ as High-Mobility Transparent Conductive Oxide. *Jpn. J. Appl. Phys.* **2007**, *46* (No. 28), L685–L687. <https://doi.org/10.1143/JJAP.46.L685>.
- (10) Calnan, S.; Tiwari, A. N. High Mobility Transparent Conducting Oxides for Thin Film Solar Cells. *Thin Solid Films* **2010**, *518* (7), 1839–1849. <https://doi.org/10.1016/j.tsf.2009.09.044>.
- (11) Powalla, M.; Paetel, S.; Ahlswede, E.; Wuerz, R.; Wessendorf, C. D.; Magorian Friedlmeier, T. Thin-film Solar Cells Exceeding 22% Solar Cell Efficiency: An Overview on CdTe-, Cu(In,Ga)Se₂ -, and Perovskite-Based Materials. *Appl. Phys. Rev.* **2018**, *5* (4), 041602. <https://doi.org/10.1063/1.5061809>.
- (12) Lee, T. D.; Ebong, A. U. A Review of Thin Film Solar Cell Technologies and Challenges. *Renew. Sust. Energ. Rev.* **2017**, *70*, 1286–1297. <https://doi.org/10.1016/j.rser.2016.12.028>.
- (13) Green, M. A.; Dunlop, E. D.; Siefert, G.; Yoshita, M.; Kopidakis, N.; Bothe, K.; Hao, X. Solar Cell Efficiency Tables (Version 61). *Progress in Photovoltaics* **2023**, *31* (1), 3–16. <https://doi.org/10.1002/pip.3646>. <https://doi.org/10.1109/JPHOTOV.2019.2937218>.
- (14) Jehl, Z.; Rousset, J.; Donsanti, F.; Renou, G.; Naghavi, N.; Lincot, D. Electrodeposition of ZnO Nanorod Arrays on ZnO Substrate with Tunable Orientation and Optical Properties. *Nanotechnology* **2010**, *21* (39), 395603. <https://doi.org/10.1088/0957-4484/21/39/395603>.
- (15) Haller, S.; Suguira, T.; Lincot, D.; Yoshida, T. Design of a Hierarchical Structure of ZnO by Electrochemistry for ZnO-Based Dye-Sensitized Solar Cells: Design of a Hierarchical Structure of ZnO by Electrochemistry. *Phys. Stat. Sol. (a)* **2010**, *207* (10), 2252–2257. <https://doi.org/10.1002/pssa.201026140>.
- (16) Peulon, S.; Lincot, D. Mechanistic Study of Cathodic Electrodeposition of Zinc Oxide and Zinc Hydroxychloride Films from Oxygenated Aqueous Zinc Chloride Solutions. *J. Electrochem. Soc.* **1998**, *154* (3) 864–874. DOI 10.1149/1.1838359
- (17) Gallanti, S.; Chassaing, E.; Lincot, D.; Naghavi, N. Influence of Thiourea Addition on the Electrodeposition of ZnO from Zinc Nitrate Aqueous Solutions. *Electrochimica Acta* **2015**, *178*, 225–233. <https://doi.org/10.1016/j.electacta.2015.07.135>.
- (18) Lincot, D. Solution Growth of Functional Zinc Oxide Films and Nanostructures. *MRS Bull.* **2010**, *35* (10), 778–789. <https://doi.org/10.1557/mrs2010.507>.
- (19) Manzano, C. V.; Philippe, L.; Serrà, A., Recent progress in the electrochemical deposition of ZnO nanowires: synthesis approaches and applications. *Crit. Rev. Solid State Mater. Sci.* **2021**, 1–34. <https://doi.org/10.1080/10408436.2021.1989663>
- (20) Guerrero, J.; Schneider, N.; Dumoulin, F.; Lincot, D.; Isci, U.; Naghavi, N.; Robert, M. Transparent Porous ZnO|Metal Complex Nanostructured Materials: Application to Electrocatalytic CO₂ Reduction. *ACS Appl. Nano. Mater.* **2023**, *6*, 10625–10636. <https://doi.org/10.1021/acsnm.3c01591>
- (21) Yoshida, T.; Zhang, J.; Komatsu, D.; Sawatani, S.; Minoura, H.; Pauporté, T.; Lincot, D.; Oekermann, T.; Schlettwein, D.; Tada, H.; Wöhrle, D.; Funabiki, K.; Matsui, M.; Miura, H.; Yanagi, H. Electrodeposition of Inorganic/Organic Hybrid Thin Films. *Adv. Funct. Mater.* **2009**, *19* (1), 17–43. <https://doi.org/10.1002/adfm.200700188>.
- (22) Liu, Y.; Xia, M.; Ren, D.; Nussbaum, S.; Yum, J.-H.; Grätzel, M.; Guijarro, N.; Sivula, K. Photoelectrochemical CO₂ Reduction at a Direct CuInGaS₂/Electrolyte Junction. *ACS Energy Lett.* **2023**, 1645–1651. <https://doi.org/10.1021/acseenergylett.3c00022>.

- (23) Costentin, C.; Robert, M.; Savéant, J.-M. Catalysis of the Electrochemical Reduction of Carbon Dioxide. *Chem. Soc. Rev.* **2013**, 42 (6), 2423–2436.
<https://doi.org/10.1039/C2CS35360A>.
- (24) Costentin, C.; Drouet, S.; Passard, G.; Robert, M.; Savéant, J.-M. Proton-coupled electron transfer cleavage of heavy-atom bonds in electrocatalytic processes. Cleavage of a C-O bond in catalyzed electrochemical reduction of CO₂. *J. Am. Chem. Soc.* **2013**, 135 (24), 9023-9031.
<https://doi.org/10.1021/ja4030148>
- (25) Boutin, E.; Merakeb, L.; Ma, B.; Boudy, B.; Wang, M.; Bonin, J.; Anxolabéhère-Mallart, E.; Robert, M. Molecular catalysis of CO₂ reduction. Some recent advances and perspectives in electrochemical and light-driven processes with Fe, Ni and Co aza macrocyclic and polypyridine complexes, *Chem. Soc. Rev.* **2020**, 49, 5772-5809.
<https://doi.org/10.1039/D0CS00218F>
- (26) Guillén, E.; Peter, L. M.; Anta, J. A., Electron Transport and Recombination in ZnO-Based Dye-Sensitized Solar Cells. *J. Phys. Chem. C* **2011**, 115 (45), 22622-22632.
<https://doi.org/10.1021/jp206698t>